SIMULATION OF IRON-CHROME-ALUMINUM ALLOY CLADDING UNDER LOCA CONDITIONS USING THE BISON FUEL PERFORMANCE CODE

R.T. SWEET, B.D. WIRTH
Department of Nuclear Engineering, University of Tennessee, Knoxville
1412 Circle Drive, Knoxville, TN 37921, USA

K.A. TERRANI
Oak Ridge National Laboratory
P.O. Box 2008, Oak Ridge, TN 37831, USA

ABSTRACT

Iron-chromium-aluminum (FeCrAl) alloys have been identified as a potential candidate for replacing currently used Zr-alloys as light water reactor (LWR) fuel cladding because they exhibit slower oxidation kinetics in high-temperature steam. This will decrease the energy release due to oxidation and slowing cladding consumption in the presence of high temperature steam, leading to increased flexibility to achieve core cooling in accident conditions. As a continuation of the development for these alloys, cladding performance during accident and transient events must be identified.

This research targets cladding behavior during accident scenarios, such as a loss-of-coolant accident in a boiling-water reactor. This is performed by modeling the integral thermo-mechanical performance of a FeCrAl-cladding fuel rod under these anticipated conditions using the MOOSE-based, finite-element fuel performance code BISON. Results from these simulations are then compared against similar results for Zircaloy, utilizing a similar fuel rod design and material-specific models for cladding burst and oxidation implemented in BISON.

1. Introduction

The goal of identifying an alternative cladding material to Zircaloy for LWR fuel systems is to improve the reactor safety during high-temperature transient conditions. In order to provide insight into how FeCrAl cladding will perform compared to Zircaloy in this environment, fuel performance code capabilities can be extended, provided that thorough constitutive models are developed and implemented (Van Uffelen et al., 2008).

Because *in-situ* testing of LWR fuel rods under accident conditions is difficult and expensive, various test reactors and transient effects programs are utilized to develop specific thermo-mechanical models of the fuel and cladding behavior. These models can be incorporated into fuel performance codes, which can then be used to screen fuel rods for failure over a range of postulated transient scenarios. Of the scenarios which are typically considered, two design basis accidents, the loss-of-coolant accident and the reactivity insertion accident, are typically investigated to ensure reactor safety (OECD, 2012).

While each of these accidents can ultimately lead to fuel failure, the target of this analysis is the cladding behavior in the high-temperature environment sustained during a potential large-break loss-of-coolant (LBLOCA) accident. In this analysis, conditions from a mitigated

LBLOCA are extended to compare the beyond design basis accident response of FeCrAl as compared to standard Zircaloy cladding.

During a loss-of-coolant accident with Zircaloy cladding, as the reactor loses its capability to cool the fuel, fuel rod temperatures begin to increase. Eventually, if this increase in temperatures is unmitigated, then the cladding will begin to 'balloon', or deform outwards, due to the pressure differential between the interior of the fuel rod and the pressure remaining in the reactor pressure vessel. If this deformation persists, cladding burst can occur during these high-temperature conditions from a combination of thermal creep and plasticity (Erbacher and Leistikow, 1987). If the temperature continues to increase further, the exothermic oxidation reaction of the Zircaloy cladding may become autocatalytic (~1204˚C). This produces large amounts of heat, consumes the cladding, and produces hydrogen gas. Within this study, the cladding performance for both FeCrAl and Zircaloy cladding during the early stage of a severe accident progression are targeted, up to temperatures where the cladding ruptures (< 1300K). Additional simulations are included which target the fuel rod behavior as the cladding temperature increases due to the oxidation reaction (< 2000K)

Traditionally, separate fuel performance codes are utilized to simulate the fuel rod behavior under steady-state, normal operating conditions and transient conditions either in conjunction with each other, or to provide a stand-alone analysis. Transitioning the state of the fuel rod from normal operation into the transient environment is necessary to evaluate the unique condition of the fuel at a variety of fuel burnups. To accomplish this, these simulation conditions contain long-term steady-state reactor operation before transitioning into the accident scenario. This allows the state of the integral fuel rod at different specified burnups to be incorporated into the transient analysis.

Simulations of Zircaloy cladding behavior under LOCA conditions have been performed using the BISON fuel performance code (Pastore et al., 2015) with the purpose of comparing modeling predictions to the REBEKA cladding burst tests (Erbacher et al., 1990). This analysis was performed using specifications from the REBEKA cladding burst test suite and demonstrate that the BISON fuel performance code has a framework in place to implement additional models and assess fuel and cladding behavior in transient conditions.

To accurately simulate the cladding behavior under a loss of coolant accident, several key models are needed. These include chemical and phase changes of the cladding alloy (such as oxidation), high temperature constitutive behavior, and cladding rupture criteria. The conditions mentioned in this analysis only consider azimuthally uniform heat transfer conditions, and, as such, utilize axisymmetric fuel rod geometries. This is an important consideration for future work targeting the effect of fuel pellet eccentricity, nonuniform temperature profiles during core reflooding, and multi-rod failure analysis (Erbacher and Leistikow, 1987).

Section 2 discusses, in detail, the construction of the constitutive models for both cladding types. This section also provides a comparison of FeCrAl cladding burst simulations in BISON against results from the ORNL Severe Accident Test Station. Section 3 includes the identification and development of the representative boundary conditions used to simulate the normal and transient reactor operation. Section 4 provides a summary of the results from the steady-state reactor operation. Sections 5 summarizes the results of the LOCA analysis up to cladding rupture and Section 6 details the results of extending these simulations by calculating the thermal solution following mechanical failure. A summary of the work performed and future model improvements is discussed in Section 7.

2. High-Temperature Constitutive Models

In order to assess the condition of the cladding materials under LOCA conditions, high-temperature (< 2000K) behavioral models were developed as needed and implemented into

BISON. These models for Zircaloy and FeCrAl include high-temperature thermal creep, plasticity, failure, and oxidation. Additionally, the models were evaluated against data from cladding burst tests to assess their accuracy.

2.1 High-Temperature Thermal Creep Model

For these simulations, both the FeCrAl and Zircaloy cladding utilize two separate models for the thermal creep calculation. These models use a separate calculation during lower temperature steady-state conditions, and under transient conditions, transition into high-temperature models.

For the FeCrAl cladding, the Arrhenius-based relationship describing the C35M thermal creep behavior is used, which is recommended for temperatures up to 870 K (Field et al., 2017). Above 900 K, a creep relation described by Saunders et al. (Saunders et al., 1997), is used. To transition between the high and low temperature creep relations, an additional Arrhenius-based relation has been fit and implemented. This transition function is used to ensure that the creep calculation remains a continuous function and does not hinder code convergence. Equation 1 shows the general form of the thermal creep equation used in these calculations. Tabulated values used in the thermal creep calculation for FeCrAl cladding are shown in Table 1.

$$\varepsilon_{c,th} = C \cdot \sigma^n \cdot \exp\left(-\frac{Q}{kT}\right) \cdot t \tag{1}$$

where C is the creep pre-exponential (s^{-1}–Pa^{-n}), σ is the effective stress (Pa), n is the stress exponent fitting parameter, Q is the creep activation energy (eV), T is the temperature in K, t is the time in seconds, and k is the Boltzmann constant ($eV\text{-}K^{-1}$). Figure 1 shows the distinct increase in the thermal creep rate corresponding to the high-temperature regime for three varying stresses. Because the same stress exponent is used at all temperatures, the stress scaling between the curves remains constant.

Table 1. Thermal Creep Parameters for FeCrAl Cladding

Cladding Temperature (K)	Creep Prefactor, A (Pa^{-n}-s^{-1})	Activation Energy, Q (eV)	Stress Exponent, n (unitless)
<= 860	2.89e-36	2.560	
860 < T < 890	2.20e-12	6.635	5.5
=> 890	5.96e-27	4.062	

Similarly, for the Zircaloy-4 cladding, the Limback thermal creep model (Limbäck and Andersson, 1996) is used up to 700 K. Above 900K, a cladding thermal creep model derived from cladding tests under LOCA conditions is used, as described by (Erbacher et al., 1982). Between these temperatures, a weighting term is used to interpolate between the different functions. The LOCA thermal creep model currently implemented in BISON takes the same form as the model for the FeCrAl (Eq. (1)). This model also takes into account the volumetric fraction of the α and β phase in the Zircaloy cladding based on the time and temperature variation rate (Pastore et al., 2015). Additionally, this calculation also includes an anisotropic reduction factor for the pure – α phase (Erbacher et al., 1982).

Table 2. High-Temperature Creep Parameters for Zircaloy-4 Cladding (Erbacher et al., 1982) [adapted from (Pastore et al., 2015)]

Zircaloy Phase	Creep Prefactor, A (Pa^{-n}-s^{-1})	Activation Energy, Q (eV)	Stress Exponent, n (unitless)
α	3.99e-32	3.33 + 2.56e-4 (T-923.15)	5.89
α-β (50%-50%)	2.51e-15	1.06	2.33
β	1.65e-22	1.47	3.78

Note: in the mixed α-β phase if the strain rate exceeds 3e-3s^{-1}, interpolation is performed directly between the individual α and β phases

Figure 1 shows the thermal creep rate for both cladding materials from 600 K – 1220 K for increasing stresses. This considers only the pure α-phase Zircaloy thermal creep constants. Zircaloy exhibits much more thermal creep at lower temperature, and this trend does persist with increasing temperature, although with a decrease in the difference between the thermal creep rates of Zircaloy versus FeCrAl. As the temperature reaches nearly 1200 K, the thermal creep rate for the FeCrAl is about an order of magnitude less than Zircaloy. This shows the Zircaloy cladding will experience much more thermal creep deformation than the FeCrAl cladding over burst relevant conditions.

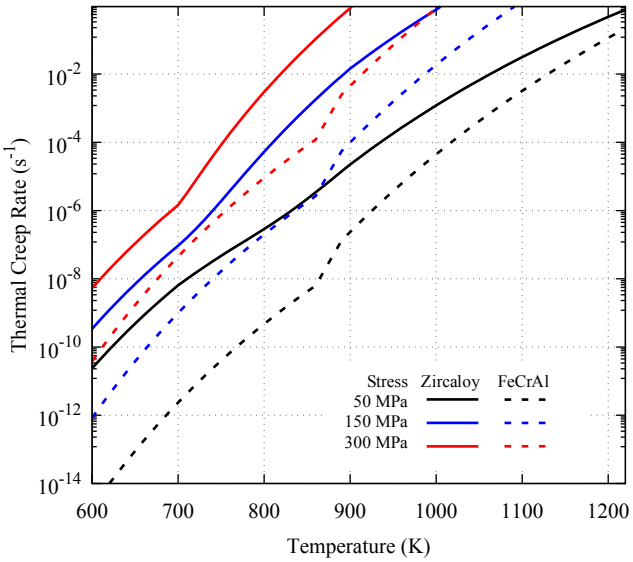

Figure 1. The thermal creep behavior for both the FeCrAl and the Zircaloy is divided into a separate low-temperature and high-temperature contribution with interpolation between the two regions.

2.2 Cladding Plasticity and Failure Models

In order to calculate the plastic deformation and assess failure of the cladding materials, isotropic plasticity models are used to define the stress-strain relationship after the material reaches the yield point. For this analysis, data from FeCrAl material testing (Maloy et al., 2016; Yamamoto et al., 2015) is used to develop a power-law strain hardening model which is implemented into BISON. The ultimate tensile strength is used as the failure criteria for the FeCrAl cladding. As the strain progresses beyond the yield point of the material, the simulations will eventually reach the failure criteria; when this stress is reached, the simulation is terminated. This is based on observations from prior burst testing experiments where very little necking occurs in the cladding before rupture (Massey et al., 2016). The yield strength and ultimate tensile strength of FeCrAl are detailed in (Yamamoto et al., 2015). Both the yield and ultimate strength begins to rapidly decrease as the temperature approaches ~2/3 of the

alloy melting temperature. For this analysis, the C35M (Rolled) properties are used to simulate the FeCrAl cladding.

In order to utilize this method of cladding failure, the uniform plastic elongation was obtained from an similar FeCrAl sample (Maloy et al., 2016) and used to derive a series of power-law strain hardening relations for the alloy at several different temperatues. These relations were implemented into BISON and interpolated to provide a more thorough description of the temperature-dependant plastic behavior of the FeCrAl cladding. This model does not consider any change in the yield strength or ultimate tensile strength due to irradiation hardening. While irradiation hardening is known to increase both the yield and tensile strength at reactor operating temperatures (Field et al., 2017), assessing the appropriate values to use during an accident is complicated by the anticipated thermal annealing of the irradiation damaged microstructure.

To demonstrate the power-law strain hardening model and FeCrAl cladding failure criteria, a rudimentary simulation of a tension test was performed in BISON for the FeCrAl alloy. This tests consists of a coarse finite-element tensile specimen where the bottom is fixed and the top of the test specimen is subject to a slowly increasing strain. This places the specimen in uniaxial tension, and the yield and subsequent failure of the material can be modeled, as shown in Figure 2. In this simulation, the tensile test was performed at four separate temperatures ranging from room temperature to the approximate cladding rupture temperature expected during a LOCA. These simulations end with assumed cladding failure at the calculated ultimate tensile strength. The results of these BISON modeled tensile tests show a decreasing yield strength and ultimate tensile strength with increasing temperature and show the variation in uniform elongation of the alloy, expected at cladding failure.

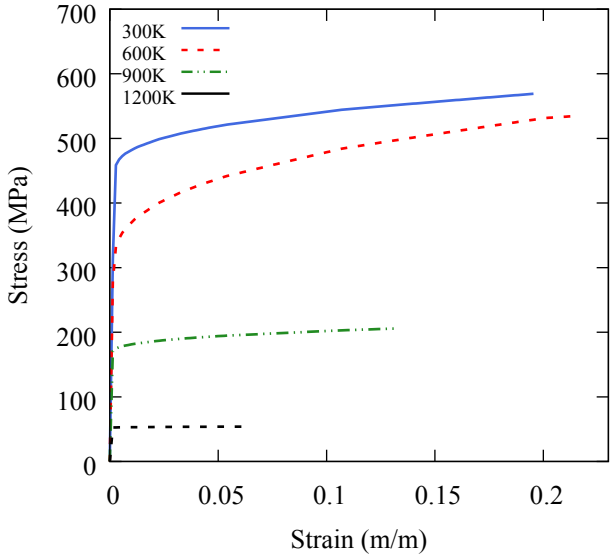

Figure 2. BISON model predictions for the stress strain response of a FeCrAl subject to a simulated tensile test, as a function of test temperature. These simulations end when the ultimate tensile strength is reached.

In order to better predict the high-temperature failure of the FeCrAl cladding, the ultimate tensile strength of the alloy was re-examined. This was motivated by a lack of data at higher temperatures where the alloy is expected to lose strength much faster than a simple linear interpolation to the melting temperature would predict. Figure 3 shows the ultimate tensile strength implemented into BISON. This shows that above 1000 K there is no data, so the expected behavior of the alloy must be used. In the first iteration of this model, the ultimate tensile strength was simply interpolated to the melting temperature where the alloy is assumed to have no remaining strength (~1773K). This results in an overprediction of the ultimate

tensile stress. Next, the ultimate tensile strength was estimated based on the high temperature performance of stainless steels, which lose much of their strength before the alloy reaches the melting temperature. This was compared against recent results generated from fitting directly to burst test data (Gamble et al., 2017), and it agrees reasonable well between 1100K -1500K. At lower temperatures (1000K – 1100K), the burst test fit predicts a slightly larger ultimate tensile strength, which may lead to a longer time before cladding rupture.

While this is an early implementation for the failure criteria of FeCrAl cladding, a more thorough examination of the material behavior at high temperatures could be made with more ultimate tensile strength data.

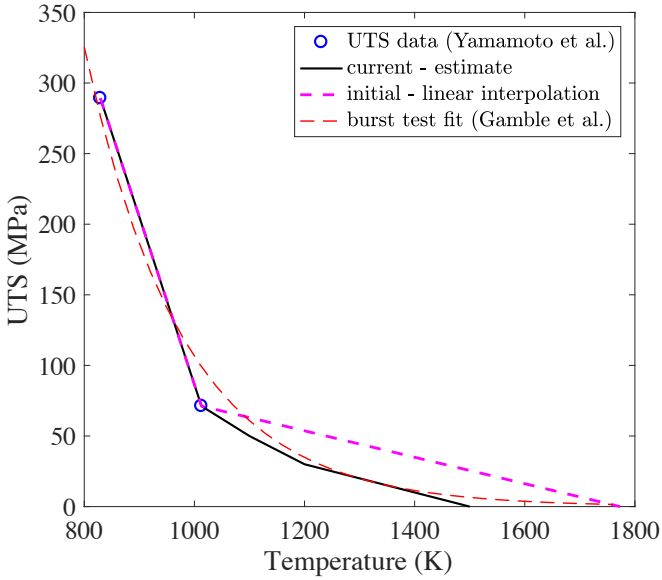

Figure 3. Ultimate tensile strength of FeCrAl as a function of temperature showing two iterations of the model implemented in BISON for high temperatures (initial versus current), compared to a fit to available data performed by Gamble and co-workers (Gamble et al., 2017) and UTS data from (Yamamoto et al., 2015).

To calculate the plastic behavior of the Zircaloy cladding, a much more thorough model, the PNNL stress-strain correlation, developed at Pacific Northwest National Laboratory for the FRAPCON fuel performance code (Geelhood et al., 2008), is currently implemented in BISON (Hales et al., 2014) and used for this analysis. This model utilizes a strain-rate dependent strain hardening model with a variable (temperature, cold work, compositions, etc.) strain hardening exponent and strength coefficient to predict the Zircaloy response at higher fuel burnups.

Failure of Zircaloy cladding is determined from burst stress data that was developed from the REBEKA burst test experiment (Erbacher et al., 1982), in addition to a strain rate failure criteria for low-stress failure. This burst stress function is shown in Equation 2, and is dependent of the cladding phase, temperature, and the fraction of oxygen dissolved into the cladding.

$$\sigma_B = a \cdot exp(-bT) \cdot exp\left(-\left(\frac{f_{wt,ox} - 0.0012}{9.5 \cdot 10^{-4}}\right)^2\right) \quad (2)$$

Where σ_B is the cladding burst stress in MPa, a and b are burst stress parameters (shown in Table 3) based on the phase of the Zircaloy, T is the temperature in K, and $f_{wt,ox}$ is the weight fraction of oxygen dissolved in the cladding. In this expression, the initial oxygen weight fraction of the cladding is assumed to be 0.0012. In BISON, the oxygen weight fraction in the cladding is calculated from the oxygen mass gain from the cladding oxidation model. As

previously mentioned, the Zircaloy phase fraction is calculated using a separate model in BISON (Pastore et al., 2015).

Table 3. Phase Dependent Burst Stress Parameters for Zircaloy-4 (Erbacher et al., 1982)

Phase	a (MPa)	b ×10^3 (K^{-1})
α	830	1.0
α-β (50%-50%)	3000	3.0
β	2300	3.0

At high temperatures, the zircaloy cladding experiences a large thermal creep strain rate which allows the alloy to undergo significant stress relaxation such that the burst stress cannot be reached. Because this model may not accurately assess the cladding failure in low-stress conditions, an additional strain-rate failure criterion ($\dot{\varepsilon_B} = 2.78 \cdot 10^{-2}\ \ s^{-1}$) is used (Hales et al., 2014; Pastore et al., 2015). It has also been suggested to include a limiting strain along with the strain rate criteria (Van Uffelen and Suzuki, 2012), and although this is not included here, it will be examined as this work is extended.

2.3 Oxidation Models

The oxidation behavior for both cladding types has been implemented into BISON in order to calculate the weight gain of oxygen in the cladding, the thickness of the oxide layer on the cladding, and the thickness of the metal consumed. For both cladding types, a low temperature and high temperature oxidation model is included.

The high temperature data for the FeCrAl cladding is based on measurements of the Kanthal APMT alloy, which have been modified using a scale factor to adjust for the alloy composition (Field et al., 2017). This work details the result of a series of oxidation tests carried out in 1200˚C steam for a variety of compositions of FeCrAl alloys, with varying chromium and aluminum content. For the expected alloy (>10% Cr 5-6% Al), a scale factor of 2.3 is used and assumed to be conservative.

In order to simulate FeCrAl in the BWR environment, data is used from an investigation of the oxidation of an Fe-13Cr-4Al alloy in hydrogen water chemistry (Terrani et al., 2016). The high temperature and low temperature relations are then connected as the high-temperature reaction is extended down to 1173K and the low-temperature is interpolated using an Arrhenius relation from the single present data point to the lowest high-temperature point. This is interpolated to the lowest temperature where alumina is expected to become the dominant oxidation layer formed (Engkvist et al., 2010; Rybicki and Smialek, 1989). Without much data in the intermediate temperature region, it is difficult to determine the accuracy of this assumption, however, the oxidation rate constants indicate that, even at elevated temperatures, much less oxidation is expected than for Zircaloy.

To simulate the Zircaloy cladding for low temperatures, linear oxidation kinetics are considered and implemented using a specific model for a boiling water reactor (Lanning et al., 1997). This model uses linear kinetics because it assumes that the transition thickness from cubic to linear scaling is negligible. It should be noted that this BWR specific model predicts significantly less mass gain than corresponding models for PWRs, consistent with the lower cladding temperatures in a BWR.

At higher cladding temperatures (>673 K) the Leistikow et al. (Leistikow et al., 1983) oxidation model is implemented as described by Pastore and Shanz, respectively (Pastore et al., 2015; Schanz, 2003). To provide a conservative estimate of the oxide formation after increasing past the normal operating temperatures, this model is extended to lower cladding temperatures than originally intended (~873K).

3. LOCA Operating Conditions

In order to simulate the LOCA, representative boundary conditions are applied to the axisymmetric fuel rod geometries described in, reviewed in Table 4. These fuel rod designs are estimates of those from a BWR/4 which have been modified due to limited data and, in the case of the FeCrAl cladded fuel rod, to account for the parasitic neutron absorption for the cladding alloy.

The postulated accident and associated conditions are derived from a study on the effect of fuel thermal conductivity on the temperature progression of the fuel and cladding during a LBLOCA in a BWR (Terrani et al., 2014). For this accident scenario, there is an assumed double-ended guillotine break in the coolant pipe between the pressure vessel and the recirculation pump isolation valve. The onset for this accident is actuated at three separate fuel burnups to determine the sensitivity of the cladding behavior to the integral fuel rod state. The power production for this fuel rod is controlled with a power history and axial power profile, while the cladding temperature is controlled by the coolant temperature and coolant heat transfer coefficient. The reactor is operated using steady state conditions until the accident is initiated at the time of 0s. Here, the recirculation pipe is assumed to be broken and the reactor is scrammed. As power in the core is reduced and the recirculation pumps slowly blowdown, the cladding temperatures initially decline. However, as the coolant flow slowly stagnates, the cladding temperatures begin to rise. The low-pressure coolant injection system is actuated at ~91s and eventually quenches the core.

Table 4. Fuel geometry specifications for 2D axisymmetric fuel performance

Cladding Material	Fuel Radius (μm)	Gap Thickness (μm)	Cladding Thickness (μm)	Fuel Length (m)	Cladding Length (m)	Enrichment (% U-235)
Zircaloy	4400	100	600	3.66	4.08	4.11
FeCrAl	4700	100	300			4.68

- This produces a total outer radius of 5100μm for both cladding types.

analyses.

In order to determine the difference in cladding performance during the unmitigated accident, these simulations do not consider the initiation of the low-pressure coolant injection system; the fuel rod temperatures are allowed to increase until cladding failure consistent with a beyond design basis accident scenario.

The power history and axial power profile used in this analysis is shown in Figure 4. The fuel rod power ramps up to steady-state operation at 20 kW/m over 100 hours and held constant until the designated burnup is reached. At the onset of the accident conditions, the reactor core is scrammed and the fuel power is reduced. Equation 3 is used to calculate the assumed power production due decay heat (El-Wakil, 1978).

$$Q_{decay} = 9.5 \times 10^{-2} \cdot Q_0 \cdot t^{-0.26} \quad (3)$$

Where Q_{decay} is the decay heat production in the fuel (kW/m), Q_0 is the steady state heat production (in this case 20 kW/m), and t is the time after the reactor scram (seconds). While this is not the most accurate calculation for decay heat production, it does provide a representative value, which, for this particular case this leads to ~ 2 kW/m after the reactor scram. The axial power profile, shown in Figure 4(b) remains static in these calculations. As discussed later, this eventually leads to a single axial length of the fuel rod which experiences considerably higher temperatures, greater burnup, and during the transient, even greater decay heat production.

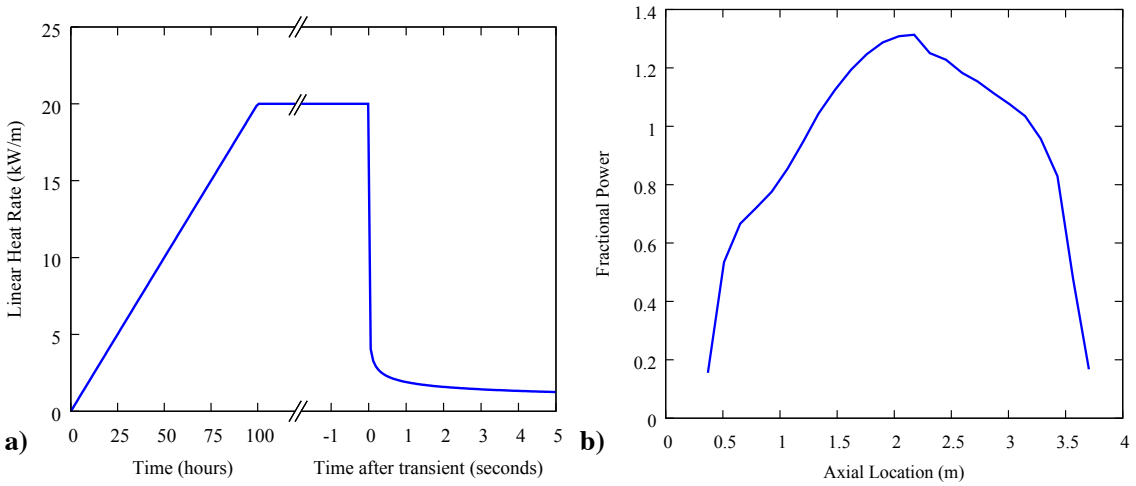

Figure 4. The power history of fuel rods in this LOCA analysis, (a) the Linear heat rate is divided into three regions: the initial ramp to operating power, constant operation at 20kW/m, and the reactor scram at the beginning of the transient conditions and the subsequent decay heat production. The axial power profile (b) is assumed to be constant for all three regions.

Pertinent reactor and fuel rod properties and typical for a BWR, are summarized in Table 5.

Table 5. Loss-of-Coolant Accident Reactor and Fuel Properties

Parameter	Value	Unit
Coolant Pressure	7.136	MPa
Initial Plenum Pressure	0.5	MPa
UO_2 Density	95%	T.D.

4. Steady-State Operation Results

For these simulations, before the onset of the transient conditions, the fuel of both cladding types is operated to three specified burnups, namely, 20 MWd/kgU, 40 MWd/kgU, and 60 MWd/kgU. This is performed to compare the accident progression and failure of both cladding types as a result of the fuel rod state (temperature, pressure gap thickness, etc.). Because a comparison of the Zircaloy and FeCrAl cladding behavior under constant operating conditions is thoroughly discussed elsewhere (Sweet et al., 2018), only condensed results are presented here.

Figure 5 shows the average fuel centerline temperature (a) and the minimum gap thickness (b) for these fuel rods up to a burnup of 60 MWd/kgU. The sharp, nearly vertical, drops in the fuel temperatures occur quickly during the postulated accident and will be discussed further in the next section. The average fuel rod temperatures remain similar for much of the simulation. There is a small deviation due to the gap closure behavior between the cladding types. The Zircaloy cladding immediately begins to creep-down, closing the gap and improving the heat transfer across the fuel rod gap. This results in a lower (~50K) average fuel centerline temperature over much of the simulated fuel burnup.

The gap closure behavior of both cladding materials is shown in Figure 5(b). Although this suggests gap closure occurs at ~13 MWd/kgU and ~27 MWd/kgU for the Zircaloy and FeCrAl, respectively, this effect is localized to the highest power region, as described by the axial power profile. This is a consequence of using a static axial power profile over the entire simulation, and concentrates the neutron flux, burnup, and temperature in a small section of the fuel rod. In this fuel rod section, the fuel expands more thermally and experiences more fuel relocation and fission product swelling. In the scope of this work, fuel relocation is

considered to be the apparent increase in the fuel diameter due to the fracture and the redistribution of fuel in the cladding tube. As well, in this location, the cladding experiences more dimensional change due to irradiation (swelling/growth) and irradiation creep deformation.

The maximum oxidation thickness that forms on the cladding surface is shown in Figure 6. The Zircaloy cladding forms ~23 μm of oxidation by the end of the simulations, while the FeCrAl forms ~4μm. As previously noted, Zircaloy cladding in the BWR environment is expected for form significantly less oxidation than in the PWR (Lanning et al., 1997). Because of the linear scaling, the oxidation layer in the Zircaloy continues to grow at a constant rate. For the FeCrAl, however, due to the parabolic kinetics associated with oxide layer formation, the growth rate diminishes with increasing thickness.

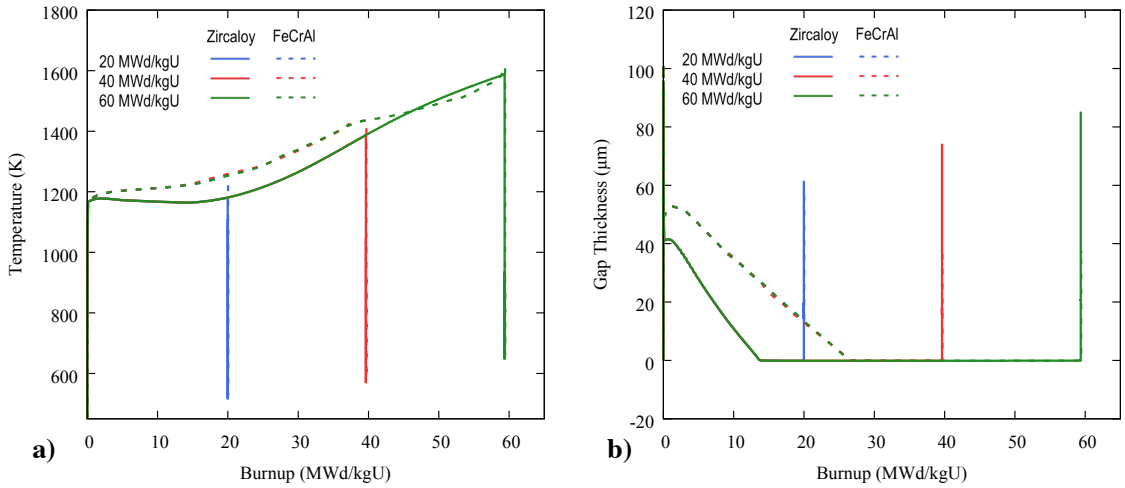

Figure 5. The average fuel temperature (a) for the FeCrAl cladded fuel rods is much larger for much of the fuel utilization. The onset of gap closure (b) occurs much sooner for the Zircaloy cladded fuel rods than the FeCrAl.

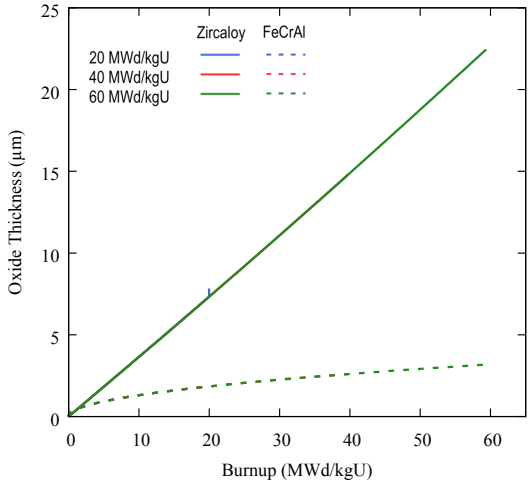

Figure 6. The maximum cladding oxidation thickness for the Zircaloy versus FeCrAl cladding, as a function of burnup.

5. LOCA Results

After the steady-state irradiation period, at a specified fuel burnup, the accident conditions are initiated based on the scenario described in Section 3, although this analysis does not initiate the low-pressure injection system at ~91 seconds after the accident. Figure 7 shows the

average fuel centerline temperature (a) and the maximum cladding temperature (b) during the transient. In these figures, the reactor is scrammed at 0s, and the reactor power then decays according to the fission product decay heat relation provided in Eq. (3). The coolant flow slowly decreases as the core recirculation pumps stop. As the coolant flow stagnates, the coolant temperatures increase, and the coolant heat transfer coefficient is decreased.

Figure 7(a) shows the variation in the fuel temperatures during the steady-state operation due to the fuel rod condition. After the reactor is scrammed, the fuel temperatures slowly decrease as the heat is removed while the coolant pumps stop. As the coolant stagnates in the core, fuel temperatures begin to rise and, eventually, converge, independent of cladding type.

The peak cladding temperatures (Figure 7(b)) show a similar trend after the accident conditions have been initialized. The cladding temperatures slowly decrease after the reactor has scrammed, reaching a minimum at ~41 seconds. This plot also shows the cladding temperatures from the TRACE simulation that actuated the low-pressure injection at approximately 91 seconds (Terrani et al., 2014). In the TRACE simulation the cladding temperatures begin to decrease at ~140 seconds as the core is re-flooded. However, in our BISON analysis the temperatures continue to increase until the cladding fails. As previously mentioned, these simulations are terminated when the burst criterion is reached. These results show progressively lower temperatures for the increasing fuel burnups. These simulations also show very similar burst times for both cladding types.

Figure 8 shows the maximum fuel cladding gap thickness (a) and the maximum cladding hoops stress (b) during the accident conditions simulated with BISON. All of the fuel rods experience gap closure by the time the accident conditions are initiated, except the FeCrAl fuel rod at the lowest burnup of 20 MWd/kgU. After the onset of the accident conditions, the fuel cools down and the coolant system pressure rapidly drops. As the fuel contracts and the cladding is expanded due to the change in pressure differential, the fuel cladding gap is reopened. For the Zircaloy, as the fuel rod temperatures begin to increase, the pressure differential between the fuel rod plenum and coolant system allow the cladding to begin rapidly expanding due to thermal creep. The FeCrAl cladding does not experience the same magnitude of thermal creep; the thermal expansion of the cladding and increase in rod internal gas pressure drive the increase in gap thickness.

Leading up to the accident scenario, the maximum cladding hoop stress (Figure 8(b)) is initially in a tensile state due to mechanical interaction between the fuel and cladding. After the onset of the LBLOCA conditions, the gap is reopened, as the reactor coolant pressure is reduced to atmospheric pressure. This generates significant hoop stresses in the cladding, as the fuel rod plenum pressure begins to increase with the fuel temperatures. In these simulations, the FeCrAl cladded fuel rods fail at much larger stresses their Zircaloy counterparts.

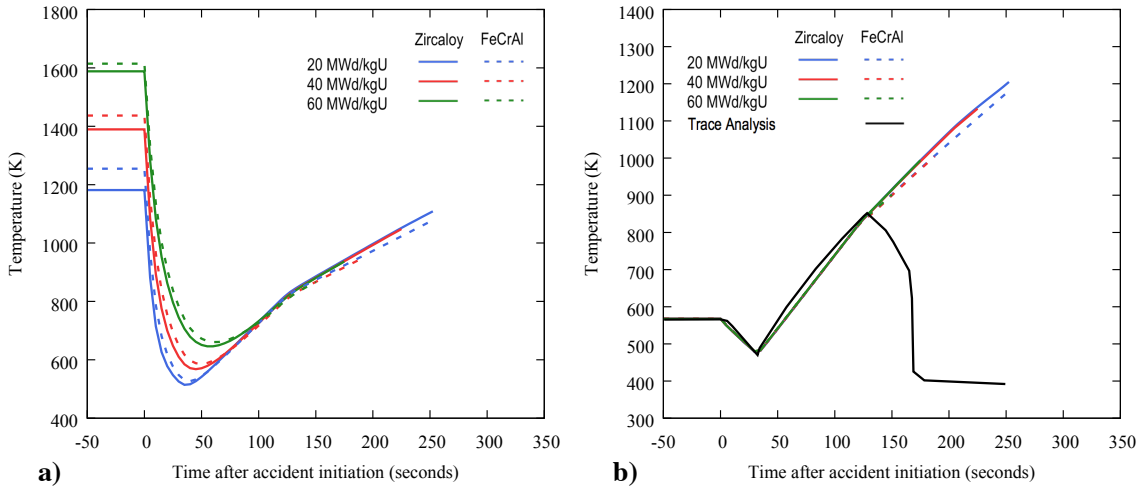

Figure 7. The maximum fuel centerline temperature (a) and the maximum cladding temperature (b) for both cladding types as a function of time after the accident. The results from the TRACE simulation are (black line) included in b) to provide a comparison.

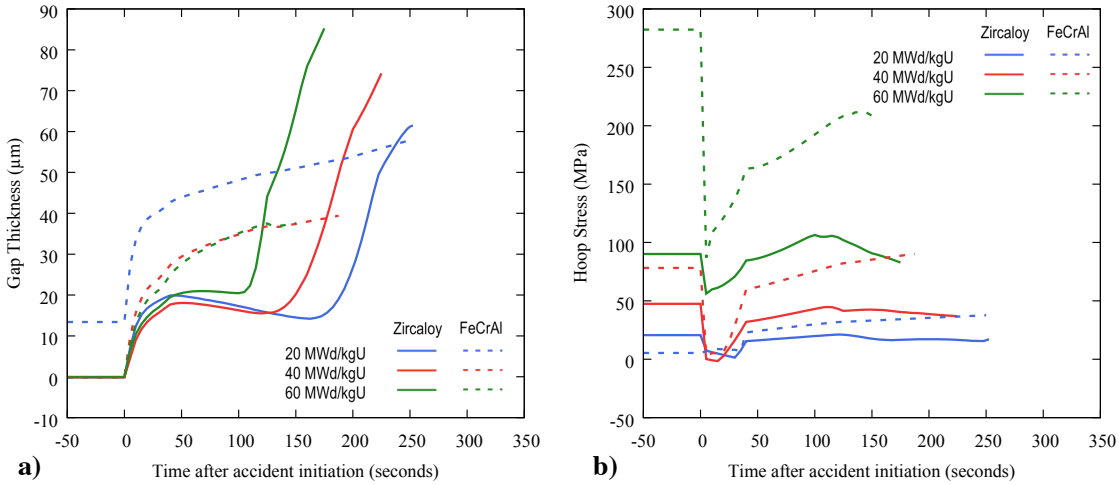

Figure 8. After the reactor is scrammed, the fuel contracts and the fuel cladding gap (a) is reopened. The Zircaloy cladding shows a much sharper increase in the gap thickness as the accident conditions progress. The maximum cladding hoop stress (b) is reduced as the accident conditions are initiated, however, as the accident progresses, the hoop stress in the FeCrAl cladding increases until failure.

These results show that the FeCrAl cladded fuel rods fail at similar times to the Zircaloy cladding, however, they fail at much larger cladding hoop stresses. The next section describes a brief analysis of the subsequent high-temperature oxidation behavior of the cladding materials.

6. Results of Extended Simulation

This analysis is extended further after the prediction of cladding rupture by considering only the thermal solution with extended time duration without operation of the emergency core cooling systems. In order to perform this analysis, the fuel and cladding mechanical strains are held constant, and the thermal solution is advanced. To simulate the post-burst behavior, the plenum pressure in the fuel rod is set equal to the coolant system pressure. This analysis is performed to elucidate the cladding oxidation behavior after burst, without the code convergence issues of high temperature mechanics. Although it is included in all simulations

in this analysis, the heat production due to the exothermic cladding oxidation reaction produces very little heat until the cladding reaches sufficiently high temperatures. These simulations are terminated when the peak cladding temperature reaches 2000 K, since by this temperature, the FeCrAl cladding would have melted.

Figure 9 shows the average fuel temperature (a) and the peak cladding temperature (b) for both fuel rods over this extended time period during the beyond design basis accident. The fuel centerline temperatures begin to deviate as the Zircaloy cladding oxidation reaction begins and continues to become autocatalytic. For these conditions, the FeCrAl cladding reaches 2000 K approximately 150 seconds later.

Figure 10 shows the cladding oxidation thickness during this extended period. The FeCrAl cladding exhibits very little additional oxidation under the transient conditions, while the Zircaloy cladding increases in a highly non-linear manner with at least an additional 20 μm of oxide thickness.

Using the calculations from the oxygen weight gain in the cladding, and assuming stoichiometric oxide formation, the hydrogen gas production per fuel rod is calculated to be ~.8g H_2 for the Zircaloy cladding and ~.05g H_2 FeCrAl cladding. Extrapolating this to an entire BWR core would yield ~ 44 kg for the Zircaloy cladding versus a much-reduced production of ~2.75 kg for the FeCrAl cladding.

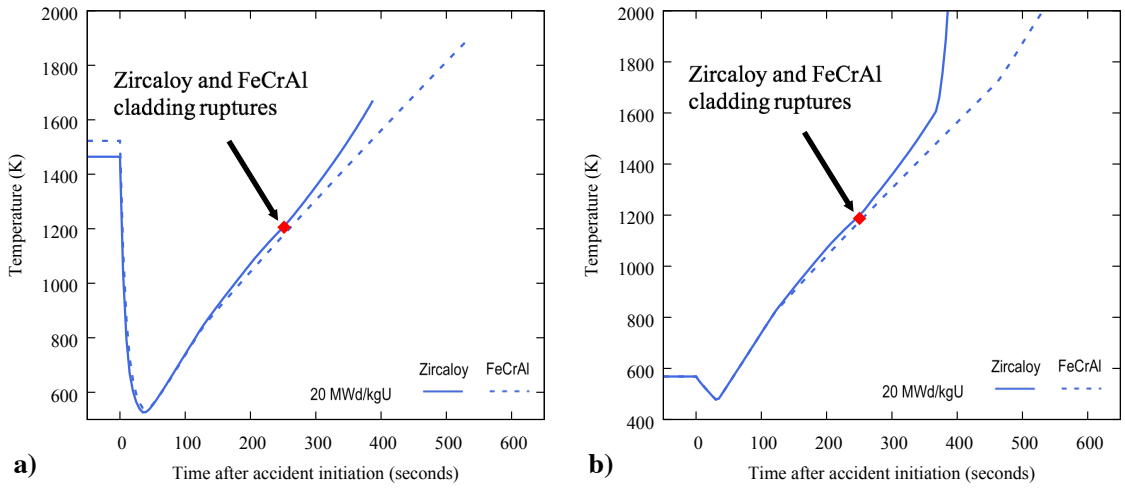

Figure 9. (a) The predicted maximum fuel centerline temperature and (b) the maximum cladding temperature for Zircaloy or FeCrAl cladded rods as a function of time following initiation of the beyond design basis LBLOCA conditions.

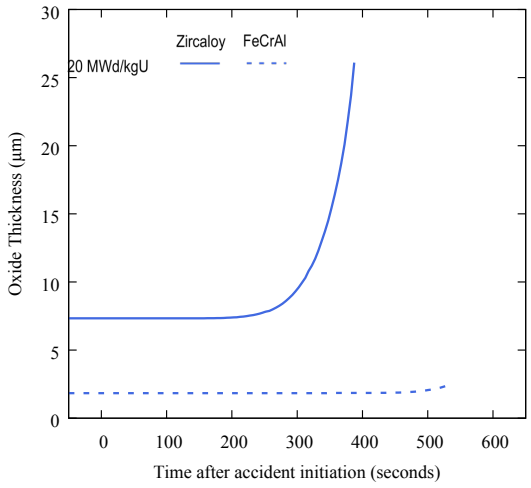

Figure 10. The maximum oxidation thickness rapidly increases for the Zircaloy after these simulations are restarted. The FeCrAl cladding, however, shows a nearly negligible increase in oxide thickness under the transient conditions.

These results provide an initial comparison of the behavior of FeCrAl and Zircaloy cladding under beyond design basis conditions. The analysis indicates that for this accident progression, the cladding materials rupture at similar times although the behavior leading up to rupture is different. The conditions of these simulations are very unique because the fuel burnup is concentrated in a small area of the fuel rod, due to the static axial power profile. This increases the heat generation due to fission product decay, and subsequently influences the mechanical behavior of the cladding in that region and the cladding oxidation. Future investigations of these cladding materials under LOCA conditions should provide a more uniform axial distribution of power over the fuel rod and improvements to the thermo-mechanical and chemical reaction models as more data becomes available.

7. Summary

This work documents initial efforts to extend the steady-state modeling capabilities established for FeCrAl cladding in the BISON fuel performance code to high temperature transient conditions. In order to compare the behavior of FeCrAl and Zircaloy cladding during a simulated a loss-of-coolant accident, high-temperature constitutive models, failure criteria, and boundary conditions were implemented.

These results show that the FeCrAl cladding will generally burst at a similar time and temperature as the Zircaloy cladding under the specific reactor operating and accident conditions that were simulated, but experience significantly larger cladding hoop stresses. As expected, the main driving force for differences in burst behavior between the various fuel burnups is the pressure differential across the cladding as the transient conditions evolve. The FeCrAl cladding thickness used in this analysis is thinner than the thickness expected to be deployed in commercial reactors, which would tend to increase the difference in cladding failure time for the FeCrAl rods during the accident. This analysis also demonstrated the ability to simulate beyond the cladding burst behavior using the thermal solution only. By extending this analysis, it was shown that because the FeCrAl cladding possesses much slower oxidation reaction kinetics there is very little increase in the oxide thickness and the cladding produces significantly less hydrogen gas.

To further enhance this analysis, additional improvements to the FeCrAl constitutive models are necessary. The development of the power law strain-hardening plasticity model consisted of a combination of different FeCrAl cladding property tests. Although these tests are conducted on similar alloys, no single test was able to provide a complete description of the

temperature-dependent plastic behavior of the FeCrAl alloy. Because of this, it is expected that the behavior of the target alloys will differ from the model that is implemented. The cladding failure models should also be subject to more thorough investigation to determine if strain-based failure models are more applicable. The current burst stress and ultimate tensile strength models lead to situations under low-stress conditions the failure time and temperature are greatly over predicted due to stress relief mechanisms in the cladding.

The operating conditions used in this analysis generate unique results because the fuel burnup is concentrated in a small area of the fuel rod due to the static axial power profile. This increases the heat generation due to fission product decay, and subsequently influences the mechanical behavior of the cladding in that region and the cladding oxidation. These simulations also do not contain the axial variation in the coolant temperature typical of a boiling water reactor. Because the temperature profile is constant axially along the fuel rod, the location of the fuel rupture is especially sensitive to the axial peaking factors. For future simulations, a combination of axial power profiles to more evenly distribute the fuel power axially over the fuel rod are expected to provide a more accurate set of conditions to model the accident progression. Coupling to a reactor systems or thermal hydraulics code would better define the cladding temperature evolution under transient conditions and would also allow evaluation of different accident scenarios.

Additionally, neither the thermal or mechanical properties of the cladding oxides have been implemented into these simulations. While the FeCrAl cladding is not expected to develop a significant oxide thickness, Zircaloy cladding is. As the cladding is oxidized and the metal is consumed, the cladding is thinned and replaced with a brittle oxide ceramic with lower thermal conductivity. Ongoing work is being performed to incorporate a discrete oxide layer directly into the finite element simulations. This may consist of either a discrete meshed oxide layer or a smeared oxide approach. A discrete oxide layer bonded to the outside of the cladding can simulate the oxide growth and cladding consumption, although there are concerns about the ability to achieve and maintain code convergence. Alternatively, a smeared oxide/cladding layer may be implemented where the material properties in the outer element of the cladding are slowly changed into the oxide. While this is computationally more efficient, accurate assessment of the growth and consumption strains will be required.

This work aims to initiate an analysis about the increase in coping time gained by using FeCrAl cladding through the use of a fuel performance code. While this work does not utilize the boundary conditions necessary to provide quantifiable results, it does showcase several areas where additional data is needed.

8. Summary

El-Wakil, M.M., 1978. Nuclear heat transport. American Nuclear Society.

Engkvist, J., Canovic, S., Hellström, K., Järdnäs, A., Svensson, J.-E., Johansson, L.-G., Olsson, M., Halvarsson, M., 2010. Alumina scale formation on a powder metallurgical FeCrAl alloy (Kanthal APMT) at 900–1,100 C in dry O 2 and in O 2+ H 2 O. Oxid Met 73, 233-253.

Erbacher, F., Leistikow, S., 1987. Zircaloy Fuel Cladding Behavior in a Loss-of-Coolant Accident: A Review.

Erbacher, F., Neitzel, H., Rosinger, H., Schmidt, H., Wiehr, K., 1982. Burst Criterion of Zircaloy Fuel Claddings in a Loss-of-Coolant Accident.

Erbacher, F., Neitzel, H., Wiehr, K., 1990. Cladding deformation and emergency core cooling of a pressurized water reactor in a LOCA. Kernforschungszentrum Karlsruhe GmbH (Germany.

Field, K.G., Snead, M.A., Yamamoto, Y., Terrani, K.A., 2017. Handbook on the Material Properties of FeCrAl Alloys for Nuclear Power Production Applications.

Gamble, K.A., Barani, T., Pizzocri, D., Hales, J.D., Terrani, K.A., Pastore, G., 2017. An investigation of FeCrAl cladding behavior under normal operating and loss of coolant conditions. J Nucl Mater 491, 55-66.

Geelhood, K.J., Beyer, C.E., Luscher, W.G., 2008. PNNL stress/strain correlation for Zircaloy. Pacific Northwest National Laboratory (PNNL), Richland, WA (US).

Hales, J., Novascone, S., Pastore, G., Perez, D., Spencer, B., Williamson, R., 2014. BISON theory manual: The equations behind nuclear fuel analysis. Fuels Modeling & Simulation Department, Idaho National Laboratory, Idaho Falls, Idaho.

Lanning, D., Beyer, C., Painter, C., 1997. FRAPCON-3: modifications to fuel rod material properties and performance models for high-burnup application. NUREG0CR-6534 1.

Leistikow, S., Schanz, G., Berg, H., Aly, A., 1983. Comprehensive presentation of extended Zircaloy-4 steam oxidation results (600-1600 deg. C).

Limbäck, M., Andersson, T., 1996. A model for analysis of the effect of final annealing on the in-and out-of-reactor creep behavior of zircaloy cladding, Zirconium in the Nuclear Industry: Eleventh International Symposium. ASTM International.

Maloy, S.A., Aydogan, E., Anderoglu, O., Lavender, C., Yamamoto, Y., 2016. Viability of thin wall tube forming of ATF FeCrAl. ; Los Alamos National Lab. (LANL), Los Alamos, NM (United States); Pacific Northwest National Lab. (PNNL), Richland, WA (United States); Oak Ridge National Lab. (ORNL), Oak Ridge, TN (United States), p. Medium: ED; Size: 35 p.

Massey, C.P., Terrani, K.A., Dryepondt, S.N., Pint, B.A., 2016. Cladding burst behavior of Fe-based alloys under LOCA. J Nucl Mater 470, 128-138.

OECD, 2012. Nuclear Fuel Safety Criteria Technical Review (Second Edition). OECD Publishing.

Pastore, G., Novascone, S., Williamson, R., Hales, J., Spencer, B., Stafford, S., 2015. Modeling of fuel behavior during loss-of-coolant accidents using the BISON code, 2015 LWR Fuel Performance Meeting—Top Fuel, Zurich, Switzerland.

Rybicki, G.C., Smialek, J.L., 1989. Effect of theθ-α-Al2O3 transformation on the oxidation behavior ofβ-NiAl + Zr. Oxid Met 31, 275-304.

Saunders, S.R.J., Evans, H.E., Li, M., Gohil, D.D., Osgerby, S., 1997. Oxidation growth stresses in an alumina-forming ferritic steel measured by creep deflection. Oxid Met 48, 189-200.

Schanz, G., 2003. Recommendations and supporting information on the choice of zirconium oxidation models in severe accident codes.

Sweet, R.T., George, N.M., Maldonado, G.I., Terrani, K.A., Wirth, B.D., 2018. Fuel performance simulation of iron-chrome-aluminum (FeCrAl) cladding during steady-state LWR operation. Nucl Eng Des 328, 10-26.

Terrani, K., Pint, B., Kim, Y.-J., Unocic, K., Yang, Y., Silva, C., Meyer, H., Rebak, R., 2016. Uniform corrosion of FeCrAl alloys in LWR coolant environments. J Nucl Mater 479, 36-47.

Terrani, K.A., Wang, D., Ott, L.J., Montgomery, R.O., 2014. The effect of fuel thermal conductivity on the behavior of LWR cores during loss-of-coolant accidents. J Nucl Mater 448, 512-519.

Van Uffelen, P., Győri, C., Schubert, A., van de Laar, J., Hózer, Z., Spykman, G., 2008. Extending the application range of a fuel performance code from normal operating to design basis accident conditions. J Nucl Mater 383, 137-143.

Van Uffelen, P., Suzuki, M., 2012. 3.19 - Oxide Fuel Performance Modeling and Simulations A2 - Konings, Rudy J.M, Comprehensive Nuclear Materials. Elsevier, Oxford, pp. 535-577.

Yamamoto, Y., Pint, B., Terrani, K., Field, K., Yang, Y., Snead, L., 2015. Development and property evaluation of nuclear grade wrought FeCrAl fuel cladding for light water reactors. J Nucl Mater 467, 703-716.